Journal Homepage: https://dergipark.org.tr/tr/pub/isibted

Isı Bilimi ve Tekniği Dergisi

Archive: https://tibtd.org.tr/dergi

Evaluating Energy and Exergy Efficiency in Solar Water Heating Systems Using the F-chart Method

Hourieh BAYRAMIAN [1, *], Huseyin GÜNERHAN [2]

[1] *EGE Üniversitesi, Fen Bilimleri Enstitüsü, Makine Mühendisliği Bölümü, Bornova, 35100, İzmir, Türkiye*
[2] *EGE Üniversitesi, Mühendislik Fakültesi, Makine Mühendisliği Bölümü, Bornova, 35040, İzmir, Türkiye*

A R T I C L E I N F O

2025, vol. 45, no.2, pp. 149-161

doi: 10.47480/isibted.1567200

Research Article
Received: 15 October 2024
Accepted: 02 July 2025

* *Corresponding Author*
e-mail: hourieh.bayramian@gmail.com

Keywords:
Analysis of exergy efficiency
Solar water heating system
F-chart method, Solar collector area
Heating load

ORCID Numbers in author order:
0000-0002-8424-9182
0000-0003-4256-2418

A B S T R A C T

This study proposes a novel method for evaluating energy and exergy performance in active solar water heating systems. It introduces new dimensionless energy and exergy efficiency numbers (EV, EV_{ex}) and solar utilization energy and exergetic ratios (F, F_{ex}) derived from the equations of the F-chart method, which are used to resize the system. Annual and seasonal variations of energy and exergy efficiencies for both the collector and the entire system, depending on their dimensionless numbers are analyzed and presented graphically. The findings reveal that as the dimensionless number of EV and EV_{ex} varies inversely proportional to the energy and exergy efficiency of the system. The system achieves a moderate energy efficiency (F = 0.57 with a 10 m^2 necessary collector area) and a relatively high exergy efficiency (F_{ex} = 0.71), indicating significant potential for usable work. While larger collector areas enhance solar and exergetic utilization, they reduce the dimensionless efficiency indicators. The study finds that collector areas between 3 and 4 m^2 strike an optimal balance, whereas a collector size of 8 m^2 is recommended for maximizing solar utilization.

Güneş Enerjili Su Isıtma Sistemlerinde Enerji ve Ekserji Verimliliğinin F-Chart Yöntemiyle Değerlendirilmesi

M A K A L E B İ L G İ S İ

Anahtar Kelimeler:
Ekserji verimliliği analizi
Güneş enerjili su ısıtma sistemi
F-chart yöntemi
Güneş kolektör alanı
Isıtma yükü

Ö Z E T

Bu çalışma, bir aktif güneş enerjisi su ısıtma sisteminin enerji ve ekserji analizi için yeni bir yöntem sunmaktadır. F-chart yönteminin denklemlerinden türetilen yeni boyutsuz enerji ve ekserji verimlilik sayıları (EV, EV_{ex}) ve güneşten yararlanma oranları, enerji ve ekserji cinsinden (F, F_{ex}) tanıtılmıştır. Bu sayılar kullanılarak sistemin boyutlandırması gerçekleştirilmiştir. Kolektör ve tüm sistemin yıllık enerji ve ekserji verim değerlerinin, boyutsuz sayılarına bağlı olarak mevsimsel değişimleri grafik halinde gösterilmiştir. EV ve EV_{ex} sayıları, sistemin enerji ve ekserji verimi miktarları ile ters orantılı bir şekilde değişim göstermektedir. Bulgular, sistemin düşük yıllık F değerlerinin yanı sıra (10 m^2 gerekli kolektör alanı ile 0,57) daha yüksek F_{ex} değerleri (0,71) gösterdiğini ve enerji dönüşümünün tam verimli olmamasına rağmen, sistemin yararlı iş potansiyeline sahip olabileceğini göstermektedir. Yüksek F_{ex} değeri ve düşük F değerleri genel enerji kullanım verimliliğini sınırlasa bile, kalan enerjinin iş yapma kabiliyetini vurgulamaktadır. Kolektör alanı arttıkça, güneşten yararlanma enerji ve ekserjetik oranları değerleri iyileşir; ancak bu değerler belirli bir noktadan sonra azalır. Daha küçük kolektör alanları birim alan başına EV ve EV_{ex} sayılarını maksimize etmede daha etkiliyken, daha büyük alanlar, F ve F_{ex} değerlerini artırır. Boyutları 3 ila 4 m^2 arasında olan kolektörler tüm ölçütler arasında bir denge kurarken, 8 m^2 civarında bir kolektör önerilmiştir.

NOMENCLATURE

A_c	collector area (m^2)
$c_{p,w}$	specific heat of water (4.179 kJ/kg. °C)
Ex_L	amount of exergy of the solar energy demand (kJ/m².day)
$Ex_{\bar{H}_T}$	exergy of the sun (kJ/m².day)
f	monthly solar utilization rate
F	annual solar utilization rate
f_{ex}	monthly exergetic fraction value
F_{ex}	annual exergetic fraction value
F_R	collector heat gain factor
$F_R{}'$	collector heat exchanger efficiency factor
$I.\bar{R}$	monthly average solar irradiance to the inclined collector surface (kJ/m².day)
$\bar{H}_T$	monthly average daily amount of solar radiation to the inclined collector surface (kJ/m^2. day)
m_{ss}	daily hot water requirement (kg/s)
$\dot{m}_w$	flow rate of water (kg/s)
n, N	number of days in a month
Q_y	monthly total heating load (kJ/day)
Q_s	Provided total energy by solar energy (kJ/m².day)
SWH	solar water heating
T_{out}	outlet domestic water temperature (°C)
T_{in}	average monthly tap water temperature (°C)
T_{col}	collector average temperature (°C)
$\bar{T}_a$	average monthly ambient temperature (°C)
$T_{required}$	desired water temperature (°C)
T_{Ref}	empirically derived reference temperature (100°C)
U_L	overall heat loss coefficient of the collector (W/m^2. °C)
$(\tau\alpha)_n$	product of the solar transmittance coefficient and solar absorption coefficient
$(\overline{\tau\alpha})$	product of the monthly average transmittance and absorption coefficient
Δt	number of seconds in a month (s)
η_{col}	collector thermal efficiency
ε	exergy efficiency

INTRODUCTION

The Paris Agreement aims to limit the rise in the Earth's surface temperature to below 2°C by achieving net-zero emissions. Currently, the average surface temperature has increased by 1.2°C compared to pre-industrial levels, resulting in more frequent heat waves and greater variability in extreme weather events (IEA, 2023). Global energy demand continues to grow rapidly due to population increases, projected to reach 10 billion by 2050 (United Nations, 2019), along with intensified economic activity in developing countries such as China, India, and Sub-Saharan Africa (Eze et al., 2024). While increasing energy demand driven by rising living standards and advancing technology has led to significant research investments to improve the efficiency of existing energy resources and meet future energy needs. Nuclear energy and fossil fuels remain the most important energy sources. However, the use of nuclear energy is constrained due to its high costs, environmental impact, and technological challenges. Similarly, the rising costs of oil and its adverse environmental effects have prompted research into the more efficient use of alternative energy sources. As traditional energy resources are depleted, sustainable solutions such as solar energy are becoming necessary. Solar energy, an infinite and clean source, is increasingly favored for its accessibility and technological simplicity (Tushar et al., 2019). Because it requires no specialized technology, solar energy is becoming increasingly widespread, enabling the development and marketing of solar technologies (Masera et al., 2023; Rosales-Pérez et al., 2023; Eze et al., 2024; Yadav and Gattani, 2022). Regions like Türkiye, which benefit from a hot, dry climate, offer great potential for utilizing solar energy to meet domestic hot water (DHW) needs. Since DHW accounts for 10% to 30% of household energy use (Kalair et al., 2022). The most common systems for providing hot water in residential buildings are solar water heating (SWH) systems (Ko, 2015). Despite their simplicity, solar heating systems are regarded as one of the most effective technologies for addressing today's environmental challenges associated with solar energy (Deutsche, 2010; Salehi et al., 2019). The optimal positioning of these systems is crucial for maximizing user benefits, particularly in large-scale applications. The level of insulation and the demand for hot water significantly influence the design process. Additionally, employing energy-efficient backup heating solutions and optimal system design can considerably lower residential water heating costs (Afzanizam et al., 2019). To enhance the energy and exergy efficiency of the system, achieve high performance, and maximize economic benefits, it is vital to understand the impacts of various components. Various methods have been developed for evaluating and designing solar energy (SE) systems, including detailed simulations and simplified procedures like the F-chart method (Duffie and Beckman, 2013; Klein et al., 1975). The F-chart method stands out as an easy and effective tool for forecasting the performance of long-term solar heating systems and is highly beneficial for improving system design, energy efficiency, and overall performance. This method considers several variables that affect thermal performance, including system characteristics like collector size, heat storage capacity, and climatic conditions. Many researchers have concentrated on theoretical and experimental investigations regarding designing systems that harness solar energy. In these studies, the F-chart method is frequently utilized to highlight energy and economic analysis. Conversely, there are some investigations in the literature evaluating solar-powered systems concerning exergy analysis (Beygzadeh et al., 2018; Mabrouki et al., 2022; Zhou et al., 2022), which consider both the quantity and quality of energy, offering a more comprehensive evaluation of system efficiency and sustainability (Hepbaşlı et al., 2019; Kalogirou et al., 2016). The F-chart method and exergy analysis are widely employed to assess the performance of solar heating systems as they consider different facets of energy utilization. To date, no research has combined the F-chart method with exergy analysis in the literature. Merging the prediction accuracy of the F-chart method with the detailed insights gained from exergy analysis can offer significant advantages, such as optimizing system components, minimizing inefficiencies, and enhancing the utilization of solar energy. Understanding the relationship between energy and exergy analysis in the context of SWH systems is important. Further exploration is necessary to effectively integrate these two approaches in the study of SWH systems.

The novelty of this paper lies in its integration of energy and exergy connections by combining exergy analysis with the F-chart method. By employing the equations from the F-chart method, we introduce dimensionless parameters. The dimensionless energy efficiency number (EV number)

evaluates the system's capacity to meet heating demands, considering available solar radiation and environmental conditions. It is calculated by dividing the energy required by the system (the heating load) by the solar energy incident on the collector area. The dimensionless exergy efficiency number (EV_{ex} number) measures the efficiency of converting solar exergy into useful output. The EV_{ex} number represents the ratio of the exergy of the heating load to the exergy of the solar energy relative to the collector area, highlighting the system's capability to convert solar energy into usable energy. Both the EV and EV_{ex} numbers evaluate the energy and exergy efficiency of the SWH systems, with the EV number indicating the system's ability to meet energy demands and the EV_{ex} number, reflecting its efficiency in exergy conversion. Additionally, the study analyzes the impacts of collector area and water heating loads on these dimensionless parameters. A theoretical SWH system tailored to the climate conditions of Mugla province in Türkiye is modeled and designed using TRNSYS simulation software. The paper proceeds as follows: Section 1 reviews related literature covering recent developments in SWH systems, the application of the F-chart method, and exergy analysis in solar thermal systems. Section 2 details the methodology, integrating the F-chart method with exergy analysis, and introduces the EV and EV_{ex} numbers. Section 3 presents and discusses the results for various collector sizes and heating loads. The study analyzes solar energy, exergetic fractions, and EV and EV_{ex} values. The conclusion summarizes important findings and their implications for the future design and optimization of SWH systems.

LITERATURE REVIEW

Ampah et al. (2024) evaluated the performance of two SWH systems across five locations in South Africa. Their analysis covered key technical like azimuth, tilt angle, solar tank volume, pump efficiency, total system flow rate, overall solar heat gain $F_R(\tau\alpha)_n$, and the thermal loss of the system $F_R U_L$. Kacia et al. (2023) conducted a study on an energy-efficient solar thermal system for Algeria's climate and determined the system's design based on an economic feasibility study. Zalamea Leon et al. (2023) applied the F-chart method to schedule energy demands for a domestic heating system using the F-chart simulation results and compared types of collectors. In another study, Esmaeili and Pourmoghadam (2023) calculated solar fraction, exergy destruction, and efficiencies of a combined cooling, heating, and power system using concentrating photovoltaic thermal collectors of various areas. Senthil et al. (2022) studied a 1.5 m^2 flat plate SWH system in South India, calculating its heat energy production for residential use, which reduces electricity consumption and conserves carbon fuel energy. Kumar Pathak et al. (2022) comprehensively review recent SWH system developments and focus on enhancing thermal performance. Rincon-Quintero et al. (2022) suggested evaluating methods to improve the efficiency of harnessing solar energy. Over the past six years, they collected data on thermodynamic parameters, exergy formulation, prevalent designs, and commonly used working fluids in flat plate solar collectors. Murugan et al. (2022) analyzed buildings' solar heating systems, examining various collectors, enhancers, and geometries for improved efficiency. The exergy efficiency curve can be a valuable tool for evaluating the exergetic performance of solar collectors. The F-chart method uses correlations from thousands of thermal performance simulations, and it is widely used for active and passive SE systems to determine the optimal design parameters, particularly for providing hot water and space heating loads, which apply to heat the medium material to temperatures not less than 20°C (Ghabour and Korzenszky, 2021). The effectiveness of an SWH system in a single-family house in Lviv, Ukraine, was evaluated using the F-chart method by Savchenko et al. (2021). Savchenko et al. (2021) evaluated the effectiveness of an SWH system in a single-family house in Lviv, Ukraine, using the F-chart method. Thangavelu et al. (2021) examined the effect of different variables to maximize the exergy efficiency of the SWH systems using TRNSYS simulation. Astudillo-Flores et al. (2021) examined the impact of solar collector orientation on energy efficiency and modeled performance under Equatorial Andean climate conditions (using the F-chart method equations). Kulkarni et al. (2020) proposed a design approach to successfully design the overall conductance of a hot water storage tank in an SWH system. Huang and Marefati (2020) investigated the energy, exergy, and environmental economics, as well as exergoeconomic analyses of various solar thermal collectors in two different cities in Iran (Tehran and Tabriz) by considering different working fluids. Afzanizam et al. (2019) found that solar energy can supply up to 78.42% of the energy required to heat domestic hot water in Ayer Keroh, making it a practical option for implementation. Hepbaşlı et al. (2019) compared traditional and passive buildings through exergy analysis at both the design and testing stages, providing valuable insights into optimizing energy efficiency. Abid et al. (2018) experimentally calculated the system's energetic and exergetic values using the exergetic product/fuel basis approach at different mass flow rates to help determine suitable building sizes. Nogueira et al. (2016) created a software tool to analyze small SWH systems, allowing users to customize designs and find cost-effective configurations. Simplified design procedures have been developed to estimate the long-term performance of heating systems using meteorological data. Various factors, including collector size and orientation, heat storage capacity, and climatic conditions, are considered when evaluating the system's thermal performance using the F-chart method (Duffie and Beckman, 2013; Kalogirou and Florides, 2016). Kushik and Ranjan (2016) estimated the energy and exergy efficiencies of SWH systems in Indian conditions by analyzing parameters such as inlet water temperature, mass flow rate, and solar radiation intensity. Meanwhile, Jafarkazemi and Ahmadifard (2013) created a thorough theoretical model for analyzing the energy and exergy of flat plate solar collectors. They discovered that the collector is where the highest exergy loss occurs in a SWH system. Various methods, ranging from detailed simulations to simple designing methods such as the F-chart method, have been developed for designing SE systems (Okafor and Akubue, 2012). Gunerhan and Hepbasli (2007) conducted an experimental exergy analysis to enhance the energy and exergy efficiencies of SWH systems. In addition, a customized exergy efficiency curve for solar collectors was proposed.

METHODOLOGY

System description

A theoretical model of an active SWH system was developed and simulated using the TRNSYS software for a residential building in Mugla province, Türkiye (37° 12' N, 28° 21' E). The proposed system uses solar energy to meet a significant portion of hot water requirements, while the conventional fossil

fuel system will meet the remaining demand. The F-chart method is employed to calculate the solar fraction value of the SWH system. The system comprised single glass flat solar collectors with a total area of 10 m^2. The collector circuit of the SWH system is estimated to have a water flow rate of 0.05 kg/s. A circulation pump with 0.16 kW power and a fluid-filled energy storage tank with a volume of 300 liters are used for the analysis, as shown in Fig 1, water with a specific heat capacity of 4.179 kJ/kg.°C is used to transfer heat fluid to the system circuit. Throughout the experiment, the ambient temperature was indicated as T_0 as recorded at its average value in the dead state, 15.4°C. In Mugla province, the interior design conditions are 20°C for winter, while the exterior design conditions are 5 °C for winter. According to the (TSE 3817, 1994) standard, if Mugla province aims to use the SWH system all year round, the collector angle relative to the horizontal ground is considered equal to the latitude angle (Karadağ, 2020).

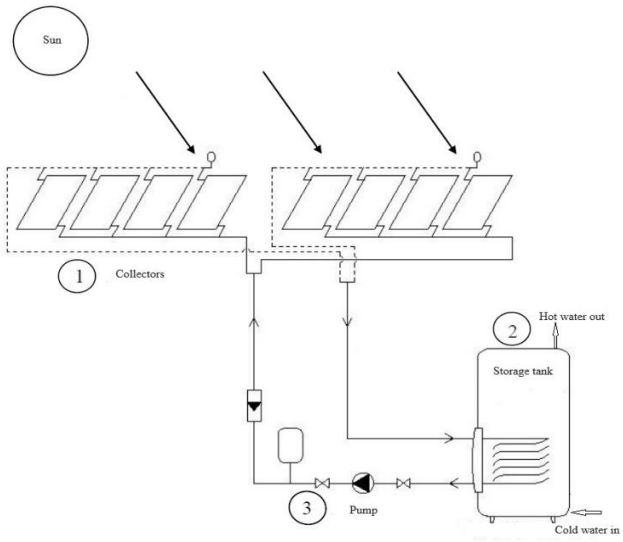

Fig. 1. The components of an active solar water heating system.

Certain assumptions and boundary conditions were considered when conducting the investigations, including maintaining a consistent water flow rate through the collector for the duration of the analysis. (b) Employing meteorological data from Mugla, Türkiye, as presented in Table 1. (c) Ensuring the piping system is well-insulated and free from heat loss. (d) The system includes the solar collector, storage tank, and pump in the analysis while assuming a linear temperature distribution for the storage tank. (e) Disregarding the effects of kinetic and potential energy on the system. According to the reference (ASHRAE Handbook, 2021) adults typically use approximately 50 liters (0.05 m^3) of hot water daily. The recommended domestic water temperature for various use points is around 60°C, but users should adjust the temperature based on the scenarios outlined in Table 2 setting the temperature at the water heater outlet to 62°C is essential to account for temperature drops between use points.

It is important to determine the appropriate size of the collector surface area based on the solar radiation values and define the monthly average solar radiation that reaches the collector's surface (Günerhan, 2005). To calculate the selected solar collector's monthly and annual performance, we need to consider the monthly total heating load for hot water (Duffie and Beckman, 2013; Jaluria, 1998). This calculation can be done using Eq. (1):

$$Q_y = m_{ss}\, c_{p,w}(T_{out} - T_{in})n \quad (1)$$

Where m_{ss} is the daily hot water requirement (kg/s), $c_{p,w}$ is the specific heat of water (4.179 kJ/kg. °C), T_{out} is the outlet domestic water temperature (°C), T_{in} is the monthly average daily tap water temperature (°C) and n is the number of days in a month. The required collector area is determined by Eq. (2):

$$A_c = \frac{Q_y}{I.\bar{R}.\eta_{col}} \quad (2)$$

Where $I.\bar{R}$ is the monthly average solar irradiance to the inclined collector surface (kJ/m^2.day) and η_{col} is the collector efficiency defined by Eq. (3):

$$\eta_k = a - b(\frac{T_{col}-T_a}{\bar{H}_T}) \quad (3)$$

Where $\bar{H}_T$ is the monthly average daily amount of solar radiation to the inclined collector surface (kJ/m^2. day), T_a is the ambient temperature (°C), and T_{col} is the collector average temperature (°C), which is obtained by Eq. (4):

$$T_{col} = \frac{T_{tap\ water}+2T_{required}}{3} \quad (4)$$

When using collector catalogs with a and b values of 0.634 and 3.636 and a collector efficiency of 0.63 (Eq. (3)), the required collector area for a single-glazed aluminum extrusion absorber with a black-painted collector is calculated to be 10 m^2 (Eq. (2)) (Günerhan, 2005; Suryanarayana and Öner Arıcı, 2003). $T_{required}$ is the desired water temperature (°C).

TRNSYS simulation approach

The dynamic simulation of the SWH system was performed using TRNSYS 18 software, a widely used and validated tool for modeling and analysis of transient thermal systems. TRNSYS allows a detailed representation of system components and operational strategies, making it an ideal choice for evaluating the seasonal performance of solar thermal systems. TRNSYS 18 software was used to simulate the entire SWH system, including the required control strategies. The software supports a wide range of applications, from simple SWH systems to complex building and equipment simulations. The primary user interface of TRNSYS is the Simulation Studio, where users can create models by dragging and connecting components from a library. The parameters of each component and system-wide simulation settings are defined in this environment (Klein, 2012; Tiwari et al., 2020).

Table 1. The average climatic conditions for Mugla province (General Directorate of Meteorology, 2021).

Parameter	January	February	March	April	May	June	July	August	September	October	November	December
Irradiance for horizontal surface (kWh/m^2)	6.28	8.918	11.43	15.491	18.841	19.259	20.725	15.407	11.221	7.746	5.862	6.423
Ambient temperature (°C)	5.4	6.2	9.0	12.8	18.0	23.4	27.0	27.0	22.2	16.5	10.6	6.7
Tap water temperature (°C)	9.6	8.5	9.6	12.3	15.8	20.4	23.8	25.5	24.4	20.5	16.4	12.2
T_{sun}	6000 K (Widén and Munkhammar, 2019)											
T_{sky}	-40 °C (Duffie and Beckman, 2013)											
$T_{collector,\ glass}$	45 °C											

Table 2. Sample hot water temperatures (ASHRAE Handbook, 2021).

Use points	Temperature (°C)
Toilet	
Handwashing	40
Shave	45
Showers	43
Commercial or institutional laundry	82 (maximum)

In this study, the TRNSYS model represents a SWH system designed for a residential building in Muğla, Turkey. The system consists of a flat plate solar collector with a total area of 10 m^2, a 300-liter hot water storage tank, and a 0.16 kW circulation pump. A control logic is also included to regulate the operation of the circulation pump depending on the temperature differences between the collector and the storage tank. Local climatic data, such as monthly average solar radiation and ambient temperatures, were input to ensure accurate boundary conditions. Input parameters such as collector optical efficiency, heat loss coefficients, flow rates, and tank heat loss factors were determined using manufacturer specifications and verified literature sources. The simulation produced outputs such as collector outlet temperature, stratification within the storage tank, thermal energy collected, pump energy consumption, and solar fraction of hot water delivered. One of the key advantages of TRNSYS is its modular and flexible structure, which allows the simulation of complex system interactions under transient conditions for an entire year. This feature has enabled a realistic representation of seasonal variations and control strategies related to the SWH system. The comprehensive modeling provided by TRNSYS provided the basis for further energy and exergy analysis using the F-chart method and the newly proposed dimensionless efficiency parameters. As shown in Fig 2 shows the actual system configuration is modeled using TRNSYS 18, and Table 3 summarizes the characteristics of each component included in the simulation.

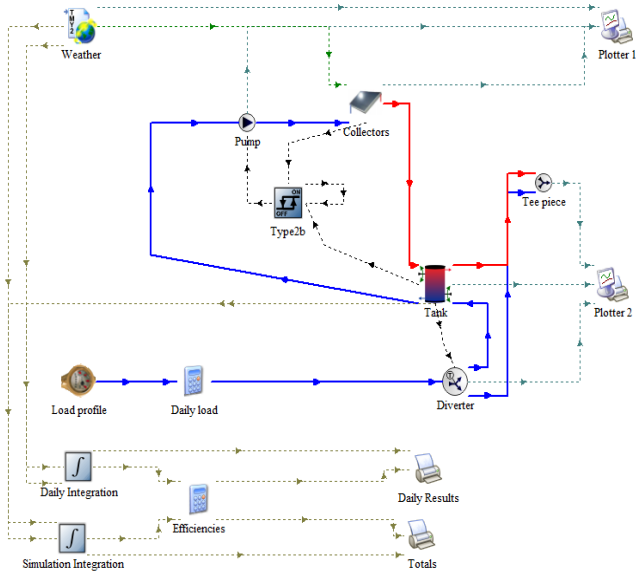

Fig 2. TRNSYS Model of the active SWH system.

F-chart method and energy analysis

The performance of liquid heating systems is determined by using the dimensionless value (f), representing the proportion of the total heating loads supplied by solar energy. The dimensionless solar fraction given by Eq. (5) is the ratio of the monthly heat load provided by the solar heating system to the total heat load. It is expressed as a function of two dimensionless numbers, X and Y (Eqs. (6)-(7)) (Astudillo-Flores et al., 2021; Okafor and Akubue, 2012):

$$f_i = 1.029Y - 0.065X - 0.245Y^2 + 0.0018X^2 + 0.0215Y^3 \quad 0 < Y < 3 \text{ and } 0 < X < 18 \tag{5}$$

$$X = F_R U_L \frac{F'_R}{F_R}(T_{Ref} - \bar{T}_a)\Delta t \frac{A_c}{L} \tag{6}$$

$$Y = F_R(\tau\alpha)_n \frac{F'_R}{F_R}\frac{(\overline{\tau\alpha})}{(\tau\alpha)_n}\bar{H}_T N \frac{A_c}{L} \tag{7}$$

Where F_R is the collector heat gain factor, U_L is the collector's overall heat loss coefficient (W/m^2.°C), Δt is the total number of seconds in a month (s), F'_R is the collector heat exchanger efficiency factor, $\bar{H}_T$ is the monthly average daily amount of solar radiation to the inclined collector surface (kJ/m^2. day), T_{Ref} is the empirically derived reference temperature (100°C), $\bar{T}_a$ is the monthly average ambient temperature (°C), A_c is the collector area (m^2), L is the monthly total heating load required for hot water and space heating (kJ), $(\tau\alpha)_n$ is the product of the solar transmittance coefficient and solar absorption coefficient, $(\overline{\tau\alpha})$ is the product of the monthly average transmittance and absorption coefficients and NIs the number of days in a month (Duffie and Beckman, 2013). The dimensionless groups F_RU_L and $F_R(\tau\alpha)_n$ are found in the efficiency curve drawn from the collector experiments. F_RU_L can be considered 4.0 W/ (m^2. °C) and 2.6 W/ (m^2. °C) for single and double glass covers, respectively. $F_R(\tau\alpha)_n$ can be taken as 0.70. The ratio F'_R/F_R is the correction ratio for various temperature drops between the collector and the tank. This value can be calculated by considering the heat exchanger efficiency as 0.95. $(\overline{\tau\alpha})/(\tau\alpha)_n$ can be taken as 0.95 for all months for single-glazed solar collectors (Duffie and Beckman, 2013; Jaluria, 1998; Suryanarayana and Öner Arıcı, 2003). In solar water and space heating systems, Eq. (8) can be used to calculate the portion of the annual heating load covered by solar energy, denoted as F.

$$F = (\sum_{i=1}^{12} f_i L_i)/(\sum_{i=1}^{12} L_i) \tag{8}$$

Where f_i and L_i is the proportion of the monthly heating load covered by solar energy, and the monthly heating load is shown below.

Table 3. The characteristics of the modeled system

Parameters	**Values**
Location: Mugla	
Latitude	37° 12' N
Longitude	28° 21' E
Altitude	670 m
Atmospheric pressure	101.28 kPa
Wind speed	30.2 m/s
Desired water temperature	60 °C
Storage hot water tank	
Volume	300 Liters
Boiler power	302 kW
Heat loss factor	1.5 kJ/h.m^2. K
Size	H/D=1
Average cold water inlet temperature	17.6 °C
Average ambient temperature	15.4 °C
Pump	
Max flow rate	30 kg/h
Max power	0.16 kW
Collector	
Total area	10 m^2
Slope	37.12
Number of collectors	1
The number of glasses covers	1
Index of refraction	1.526
ε, glass diffusivity	0.92
α, glass transmittance	0.92
Working fluid	Water
η_o, Collector optical efficiency	0.75
Heat loss coefficient	5 W/m^2. K

Exergy analysis equations

The thermal efficiency of the solar collector can be defined as Eq. (9) (Gunerhan and Hepbasli, 2007):

$$\eta_{col} = \frac{\dot{Q}_u}{A_c \bar{H}_T} \quad (9)$$

The instantaneous usable energy collected by the solar collector is given by Eq. (10):

$$\dot{Q}_u = \dot{m}_w c_{p,w}\left(T_{w,out} - T_{w,in}\right) \quad (10)$$

Where $\dot{m}_w$ is the water flow rate (kg/s), $T_{w,out}$ is the outlet temperature of water from the collector to the storage tank (K) and $T_{w,in}$ is the inlet temperature of water from the storage tank to the collector (K).

The exergy efficiency of the solar collector can be expressed as the ratio of helpful exergy delivered to the exergy absorbed by the solar collector, Eq. (11) (Gunerhan and Hepbasli, 2007):

$$\varepsilon_{collector} = \frac{\dot{E}x_{collector}}{\dot{E}x_{sun}} \quad (11)$$

The exergy absorbed by the solar collector can be expressed as Eq. (12) (Thangavelu et al., 2021):

$$\dot{E}x_{collector} = \dot{m}_w c_{p,w}\left[\left(T_{w,out} - T_{w,in}\right) - T_0 \ln\left(\frac{T_{w,out}}{T_{w,in}}\right)\right] \quad (12)$$

The exergy efficiency of the SWH system can be expressed as the ratio of the output exergy and the exergy from the sun Eq. (13) (Thangavelu et al., 2021):

$$\varepsilon_{SWH} = \frac{\dot{E}x_{out}}{\dot{E}x_{sun}}$$

$$\varepsilon_{SWH} = \frac{\dot{m}C_p\left[\left(T_{w,out} - T_{w,in}\right) - T_a\left(ln\frac{T_{w,out}}{T_{w,in}}\right)\right]}{AI_T\left(1+\frac{1}{3}\left(\frac{T_0}{T_g}\right)^4 - \frac{4T_0}{3T_g}\right) + W_{pump}} \quad (13)$$

Where $\dot{m}$ is the mass flow rate of water (kg/s), T_a is the ambient temperature (K), $T_{w,out}$ and $T_{w,in}$ are the system's out and in water temperatures, respectively (K). Considering that 0.16 kW power of the circulation pump is directly transferred to the system (assuming that there is no thermal loss); To find the temperature of the flow circuit just before the circulation pump, the power of the circulation pump, Eq. (14) is used. The temperature of the flow circuit immediately after the circulation pump is known and is the collector inlet temperature.

$$\dot{W}_{pump} = \dot{m}C_p\left(T_{pump,out} - T_{pump,in}\right) \quad (14)$$

Meanwhile, the exergy from the sun can be derived as Eq. (15) (Thangavelu et al., 2021):

$$\dot{E}x_{sun} = \bar{H}_T\left[1 + \frac{1}{3}\left(\frac{\bar{T}_a}{T_g}\right)^4 - \frac{4}{3}\left(\frac{\bar{T}_a}{T_g}\right)\right] \quad (15)$$

Where T_g is the solar radiation temperature (6000 K).

Derivation of newly defined dimensionless numbers using equations of the F-chart method with a unique mathematical approach

The system receives most of its energy input from solar radiation absorbed by the absorber plates. The exergy of a heat transfer flow ($\dot{E}x_{heat}$) is determined by Eq. (16), which depends on the reference temperature (T_{Ref}) (Jafarkazemi and Ahmadifard, 2013).

$$\dot{E}x_{heat} = \dot{Q}\left(1 - \frac{T_0}{T}\right) \quad (16)$$

Since the exergy of heat energy is usually modeled by the ambient temperature, the exergy of the monthly heating load, Ex_L (kJ/m².day) required for hot water supply and space heating can be expressed in terms of the reference temperature, T_{Ref}(373.15 K) and the monthly average ambient temperature, $\bar{T}_a$(K) as given by Eq. (17):

$$Ex_L = L\left(1 - \frac{\bar{T}_a}{T_{Ref}}\right) \quad (17)$$

Mentioning Eq. (16), the exergy amount of the sun is calculated from Eq. (18) (Gunerhan and Hepbasli, 2007):

$$Ex_{\bar{H}_T} = \bar{H}_T\left[1 + \frac{1}{3}\left(\frac{\bar{T}_a}{T_g}\right)^4 - \frac{4}{3}\left(\frac{\bar{T}_a}{T_g}\right)\right] \quad (18)$$

The F-chart approach involves using two empirical dimensionless numbers to calculate the monthly consumption rates of solar energy. X represents the ratio of collector losses to heating loads, while Y relates to the ratio of absorbed solar radiation to heating loads (Eqs. (6)-(7)) (Günerhan, 2005). Exergy is a term used to measure the usable energy potential within each system. Exergy loss or destruction is the irreversible energy loss caused by heat transfer and friction. The ratio of the exergy loss of the system to the exergy amount of the heating load provided by the system, X_{ex} is given by Eq. (19). At the same time, Y_{ex} (Eq. (20)) is defined as the ratio of the exergy of the absorbed solar radiation to the exergy of the heating load provided by the system. By using these two dimensionless values, the exergetic solar fraction can be determined (Eq. (21)). F_{ex} is the ratio of the amount of exergy provided by solar energy to the total exergy demand, and the annual exergetic fraction value F_{ex} is calculated by Eq. (22):

$$X_{ex} = F_R U_L \frac{F'_R}{F_R}\left(T_{Ref} - \bar{T}_a\right)\Delta t \frac{A_c}{Ex_L} \quad (19)$$

$$Y_{ex} = F_R(\tau\alpha)_n \frac{F'_R}{F_R}\frac{(\overline{\tau\alpha})}{(\tau\alpha)_n} Ex_{\bar{H}_T} N \frac{A_c}{Ex_L} \quad (20)$$

By considering Eqs. (6)-(7)-(17), we can express F_{ex} as Eg. (21):

$$f_{ex,i} = 1.029\, Y_{ex} - 0.065\, X_{ex} - 0.245\, {Y_{ex}}^2 + 0.0018\, {X_{ex}}^2 + 0.0215\, {X_{ex}}^3 \quad (21)$$

$$\mathrm{F}_{ex} = \left(\sum_{i=1}^{12} f_{ex,i} Ex_{L,i}\right)/\left(\sum_{i=1}^{12} Ex_{L,i}\right) \quad (22)$$

Dimensionless energy and exergy efficiency numbers

The dimensionless exergy efficiency number is denoted as EV_{ex} is calculated by normalizing the given X_{ex} (Eqs. 19 - 20) by the average ambient temperature relative to a reference temperature ($\frac{\bar{T}_a}{T_{Ref}}$) and subsequently deriving $\frac{Ex_L}{Ex_{\bar{H}_T} A_c} * \frac{\bar{T}_a}{T_{Ref}}$ expressed as Eq. (23). This normalization

helps compare thermal properties across different systems or conditions, accounting for environmental influences on heating efficiency.

$$X_{ex} = F_R U_L \frac{F'_R}{F_R}\left(T_{Ref} - \bar{T}_a\right)\Delta t \frac{A_c}{Ex_L}\frac{T_{Ref}}{\bar{T}_a}$$

$$Y_{ex} = F_R(\tau\alpha)_n \frac{F'_R}{F_R}\frac{(\overline{\tau\alpha})}{(\tau\alpha)_n} Ex_{\bar{H}_T} N \frac{A_c}{Ex_L}\frac{T_{Ref}}{\bar{T}_a}$$

Dimensionless exergy efficiency number:

$$\frac{Ex_L}{Ex_{\bar{H}_T} A_c} * \frac{\bar{T}_a}{T_{Ref}} = EV_{ek} \quad (23)$$

The data from Table 4 was used to calculate the annual fraction of the total heating load supplied by solar energy (F) and the annual exergetic fraction value (F_{ex}) for different collector areas (shown in Fig 5) using equations (8)-(22). The dimensionless exergy number is an important tool for evaluating the thermodynamic performance of a system, as it provides a valuable measure of the maximum possible exergy. Likewise, by multiplying the given X and Y equations by $\frac{\bar{T}_a}{T_{Ref}}$ and deriving $\frac{L}{\bar{H}_T A_c} * \frac{\bar{T}_a}{T_{Ref}}$ The dimensionless energy number, denoted as EV, can be obtained as Eq. (24):

$$X = F_R U_L \frac{F'_R}{F_R}(T_{Ref} - \bar{T}_a)\Delta t \frac{A_c}{L}\frac{T_{Ref}}{\bar{T}_a}$$

$$Y = F_R(\tau\alpha)_n \frac{F'_R}{F_R}\frac{(\overline{\tau\alpha})}{(\tau\alpha)_n} \bar{H}_T N \frac{A_c}{L}\frac{T_{Ref}}{\bar{T}_a}$$

Dimensionless energy efficiency number:

$$\frac{L}{\bar{H}_T A_c} * \frac{\bar{T}_a}{T_{Ref}} = EV \quad (24)$$

Regarding the F-chart method, the portion of energy demand provided by solar energy (f) is defined. At the same time, the exergetic fraction value (f_{ex}) denotes the portion of the water heating exergy demand is provided by solar energy, as defined in Eqs. (25)-(26) (Savchenko et al., 2021):

$$f = \frac{Q_S}{L} \quad (25)$$

$$f_{ex} = \frac{Q_S}{Ex_L} \quad (26)$$

Where Q_s is the definition of the total energy provided by solar energy (kJ/m^2.day).

EV and EV_{ex} numbers are critical dimensionless parameters that measure the efficiency of solar energy in meeting the heating demand of the system, considering the available solar radiation and ambient conditions. The EV number is calculated by dividing the energy required by the system, i.e., the heating load, by the amount of solar energy incident on the collector area. Low EV values indicate high solar utilisation efficiency, while high EV values indicate low solar utilisation and insufficient solar energy to meet the energy demand of the system. On the other hand, EV_{ex} number shows the ratio of the exergy amount of the heating load to the exergy amount of the solar energy according to the collector area. The EV_{ex} number provides a dimensionless measure of the performance of the solar heating system, considering both the exergy conversion efficiency and the effect of ambient temperature. The EV_{ex} number peaks in late winter and pre-summer, while the exergy efficiency of the collector peaks in early summer. EV and EV_{ex} numbers are linked to the overall energy and exergy performance. In the study, the annual energy and exergy efficiency values of the collector and the whole system, as well as seasonal changes depending on the dimensionless numbers are shown graphically. The number of EV and EV_{ex} varies proportionally with the energy and exergy efficiency of the system.

RESULT and DISCUSSION

Fig 3 and Fig 4 show the average outlet collector temperature and the outlet storage tank top and bottom temperatures (based on TRNSYS simulation). The outlet collector temperature peaks at around 335 K in July and August, then drops to 310 K by December. A solar thermal collector system typically follows this pattern: higher temperatures in summer due to increased solar irradiance and lower temperatures in winter due to reduced solar irradiance. The temperature at the top of the outlet storage tank ranges between 300 K and 330 K, peaking in July and August, while the temperature at the bottom of the tank remains between 270 K and 290 K. Both temperatures are higher in summer and lower in winter, indicating effective seasonal storage and stratification within the tank.

The peak collector outlet temperature of around 335 K (62°C) in July and August is similar to values reported by Kumar et al. (2021), who observed a peak of 66°C in Indian climates using TRNSYS modeling. This confirms the seasonal consistency in solar thermal system outputs under comparable radiation levels. The observed stratification between 270 K and 330 K is consistent with the findings of Savchenko et al. (2021), who also reported stable top-bottom temperature differences in single-family residential solar storage tanks, indicating effective thermal layering. Table 4 summarizes the annual energetic and exergetic solar fractions calculations for the collector area of 10^2 using Eq. 5-8 and 16-22. Based on Table 4, the annual fraction of the total heating load supplied by solar energy (F) Moreover, the annual exergetic fraction value (F_{ex}) was calculated using Eqs. (5)-(22) for various collector areas (Fig 5).

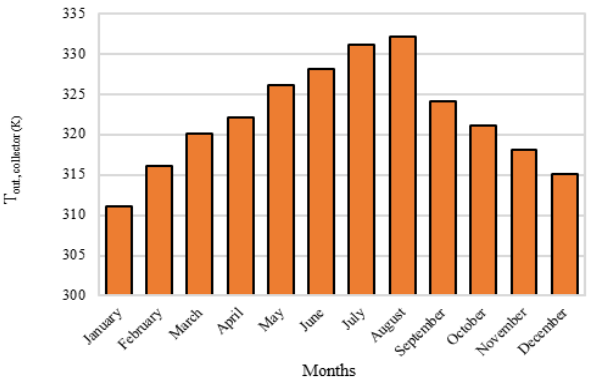

Fig. 3. The average collector outlet temperature.

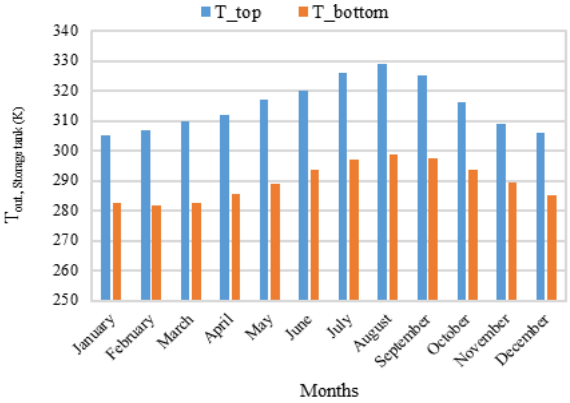

Fig. 4. The top and bottom temperatures of the storage tank.

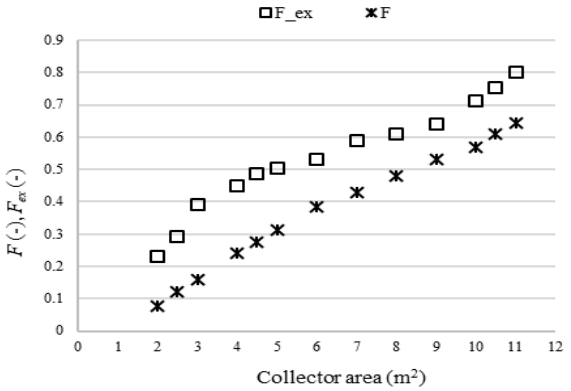

Fig. 5. The annual solar fraction (F) and exergetic solar fraction (F_{ex}) values for different collector areas.

According to Fig 5, the solar utilization ratio is relatively low, while the exergetic ratio values are relatively high. The annual F and F_{ex} values for the required 10 m² collector area are calculated as 0.57 and 0.71, respectively. These results show that the system cannot fully convert the collected energy into useful energy (low F_{ex}) but has a significant potential for usable energy (high F_{ex}). The F value expresses the solar utilization rate in terms of energy and uses local temperature data. In contrast, the F_{ex} value expresses the solar utilization rate in terms of exergy and considers solar temperature and ambient temperature in this calculation. In other words, it shows the maximum work potential that can be obtained when the sun is fully utilized. Although some energy conversion losses occur, the remaining energy can be used efficiently. Exergy not only measures useful energy but also evaluates its efficiency. A high F_{ex} indicates that the remaining energy is capable of productive work. However, low energy efficiency (F) means that there may be limited opportunities to exploit this exergy potential. The annual solar utilization rate (F = 0.57) aligns well with Savchenko et al. (2021), who reported a value of 0.39 in cooler climates with lower radiation. Our higher F_{ex} value of 0.71 compares favorably with that of Thangavelu et al. (2021), who reported 0.60–0.73 for tropical locations with flat-plate collectors. To obtain the defined dimensionless numbers, Eqs. (25) and (26) were used, and the results throughout the year are presented in Table 5. The graphic in Fig 6 shows the variation of EV compared to EV_{ex}.

Table 4. The calculations of the monthly energy and exergetic solar fraction values are based on the heating load and exergy of the heating load amounts (required water temperature of 60°C).

Months	Number of days (-)	$\bar{T}_a$ (°C)	$\bar{H}_T$ (kJ/m².day)	L (kJ)	f (-)	fL (kJ)	$\overline{Ex}_{\bar{H}_T}$ (kJ/m². day)	Ex_L (kJ)	f_{ex} (-)
January	31	5.4	9505.9	3394996	0.339	1152398.181	8917.499509	860484.49	0.595
February	28	6.1	12086.4	3130820	0.430	1345456.191	11336.39064	787655.55	0.651
March	31	8.2	12083.5	3394996	0.440	1494644.247	11328.0322	835015.6	0.665
April	30	12.6	13083.5	3116190	0.509	1585149.414	12252.72019	729706.15	0.769
May	31	17.5	15508.1	2993298	0.646	1934054.864	14506.47752	661632.07	0.798
June	30	22.6	17009.5	2608320	0.764	1991501.806	15891.63133	540896.88	0.808
July	31	26.0	17569.3	2474978	0.834	2063305.617	16401.36817	490699.6	0.873
August	31	25.9	18084.6	2364835	0.875	2068754.655	16882.81506	469495.78	0.902
September	30	21.5	16753.5	2357526	0.800	1886449.324	15656.55053	495835.58	0.812
October	31	15.8	14332.9	2788785	0.643	1728348.274	13412.59426	606569.84	0.794
November	30	10.9	11410.0	2859120	0.465	1329120.051	10689.79455	682531.55	0.627
December	31	7.3	9245.0	3226542	0.329	1062799.879	8668.845765	801363.76	0.50
		Total:	13889.35	36423859		19641982.502	155944.7197	7961886.9	

Table 5. The calculations of monthly dimensionless energy and exergy numbers (EV, EV_{ex}) using the heating load and exergy of the heating load amounts.

Months	$\bar{T}_a$ (K)	$\bar{H}_T$ (kJ/m². day)	L (kJ)	Ex_L (kJ)	$Ex_{\bar{H}_T}$ (kJ/m². day)	EV (-)	EV_{ex} (-)
January	278.6	9505.9	3394996	860484.49	8917.5	26.66	7.20
February	279.3	12086.4	3130820	787655.55	11336.391	19.39	5.20
March	281.4	12083.5	3394996	835015.6	11328.032	21.18	5.56
April	285.8	13083.5	3116190	729706.15	12252.720	18.25	4.56
May	290.7	15508.1	2993298	661632.07	14506.478	15.03	3.55
June	295.8	17009.5	2608320	540896.88	15891.631	12.15	2.70
July	299.2	17569.3	2474978	490699.6	16401.368	11.29	2.40
August	299.1	18084.6	2364835	469495.78	16882.815	10.48	2.23
September	294.7	16753.5	2357520	495835.58	15656.551	11.11	2.50
October	289	14332.9	2688785	606569.84	13412.594	14.53	3.50
November	284.1	11410.0	2859120	682531.55	10689.795	19.07	4.86
December	280.5	9245.0	3226542	801363.76	8668.846	26.23	6.95

The average ambient temperature and daily solar radiation on a horizontal surface exhibit distinct seasonal patterns, peaking in July and August and reaching their lowest levels in December and January. Similarly, the monthly variable water heating loads display marked fluctuations throughout the year, with the highest loads observed in January and the lowest in September (Table 5). EV and EV_{ex} also demonstrate seasonal differences, showing the highest values in January and the lowest in August and September. Fig 6 accompanying Table 5 illustrates a positive correlation between EV and EV_{ex} indicating a direct relationship between the two as measures of SWH system efficiency. Our dimensionless energy and exergy numbers show a positive correlation, consistent with Gunerhan and Hepbasli (2007), who demonstrated that as thermal load increases, EV and EV_{ex} values follow a similar trend. This supports the effectiveness of dimensionless analysis for SWH system design. Calculations were performed for a year at different collector areas, and the variations of EV and EV_{ex} are shown in Fig 7 (a) and (b).

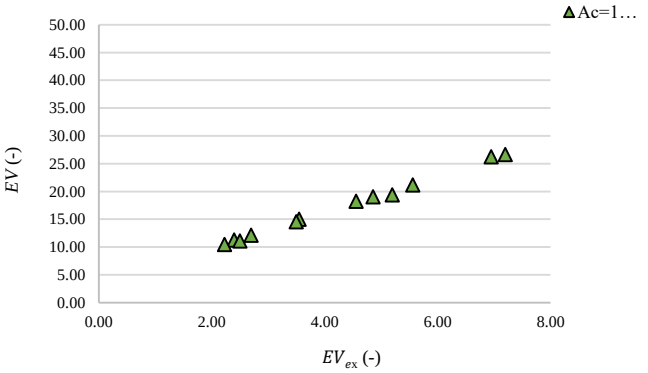

Fig. 6. Dimensionless energy number (EV) versus the exergy number (EV_{ex}).

Fig 7 shows EV and EV_{ex} decrease by increasing the collector area. This indicates that larger collector areas can improve the performance of solar thermal systems and meet more heating demand than smaller collector areas. These findings have significant implications for the design and performance of solar thermal systems, suggesting that adjusting the collector area can enhance the system's efficiency. It is important to note that the results are based on calculations performed over a year, and their validity may vary depending on location and climate conditions. Further studies are necessary to investigate the long-term performance of solar thermal systems with varying collector areas in different locations. The decline in EV and EV_{ex} with increasing collector area agrees with the trends found by Kumar et al. (2021), who also showed that larger areas improve solar utilization but reduce per-area efficiency. This trade-off is well documented in solar optimization studies.

The variation of F, F_{ex}, EV and EV_{ex} values are shown in Fig 8, while evaluating the seasonal performance of the systems, it is predicted that it will enable the design of more efficient systems in terms of both energy and exergy. From the graphs, it is possible to determine the collector area where F, F_{ex}, EV and EV_{ex} reach the optimum values. The graphs will clearly show the optimum collector area to achieve the best balance between energy and exergy efficiencies under varying seasonal conditions. The analysis shows that the EV and EV_{ex} values are maximized with smaller collector areas, while the F and F_{ex} values improve with larger areas, indicating a state of equilibrium. Larger collector areas contribute positively to achieving higher F and F_{ex} values, while smaller collector areas are more effective in maximizing the EV and EV_{ex} values. A collector area of about 3 to 4 m^2 provides a balanced solution, reaching satisfactory levels for EV and EV_{ex} values while maintaining reasonable values for F and F_{ex}. However, if the primary objective is to maximize the F and F_{ex} values, a larger collector area of about 8 m^2 is recommended. Consequently, larger collector areas are advantageous when the F value is a priority. Smaller collector areas are more effective for optimizing the EV per unit area and EV_{ex} values. Therefore, a medium-sized collector area is recommended for a balanced performance between F, F_{ex}, EV and EV_{ex} values. These results mirror the findings of Astudillo-Flores et al. (2021), who observed that smaller collector areas maximize EV and EV_{ex}, while larger areas improve F and F_{ex}. Our recommendation of a 3–4 m^2 area for balance is in line with their conclusions for equatorial climates.

Fig 9 demonstrates changes in the annual energetic and exergetic solar energy utilization rates (defined dimensionless parameters F, F_{ex}, EV and EV_{ex}) at various water heating loads (ranging from 1 to 8 GJ) with a collector area of 10 m^2.

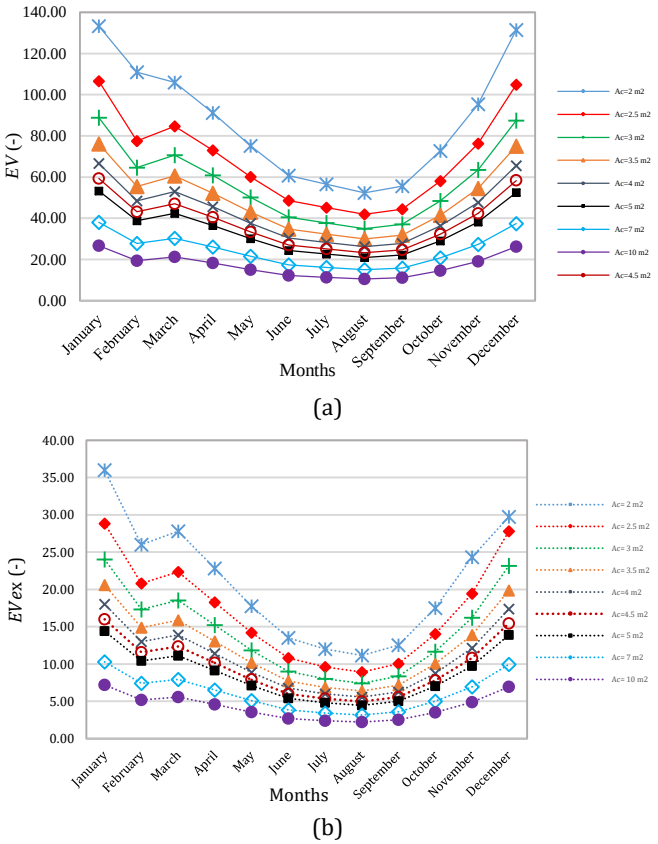

Fig. 7. The annual variations of (a) EV and (b) EV_{ek} in different collector areas.

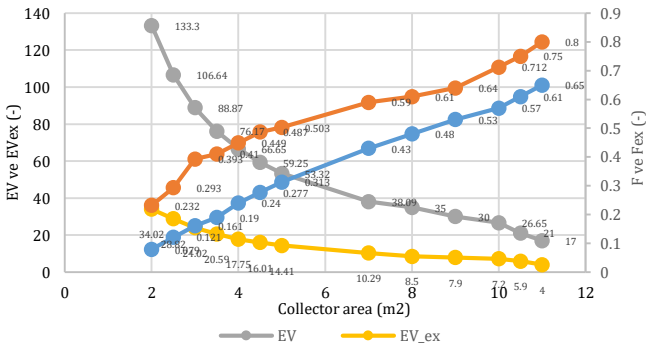

Fig. 8. Variation of F, F_{ex}, EV and EV_{ex} values for different collector areas.

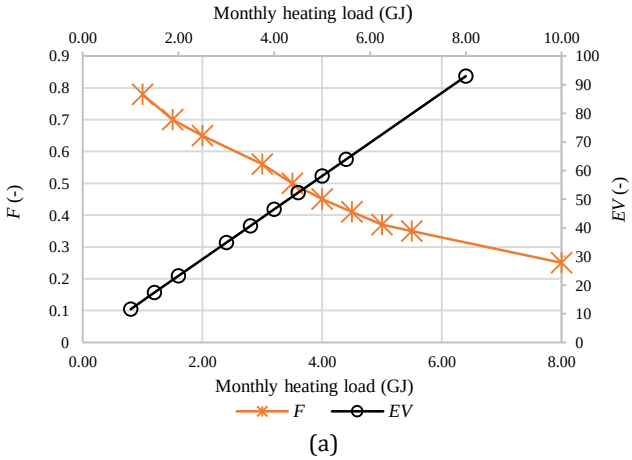

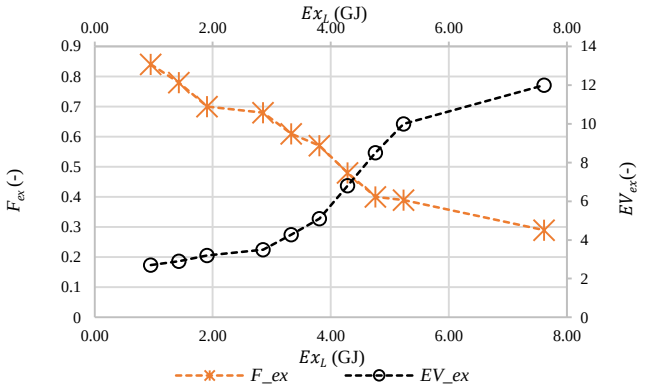

(b)

Fig. 9. Changes in the (a) energetic and (b) exergetic solar energy utilization rates at heating loads ranging from 1 to 8 GJ.

Fig 8 shows that F and F_{ex} decrease as the heating load increases, while EV and EV_{ex} increase. The exergetic utilization rate is always lower than the energetic utilization rate. Graphs show that at a heating load of 1 GJ, F is 0.78 while EV is 11.62. However, at a heating load of 8 GJ, F and EV are 0.25 and 92.97, respectively. The exergy analysis yielded similar trends. These results indicate that the dimensionless parameters increase the water heating load, leading to insufficient solar energy to meet the demand. The decrease in the utilization rates for solar energy can be attributed to changes in the ratio of solar energy utilized to meet the heating demand, resulting from changes in the collector area and heating load. The observed decrease in F and increase in EV_{ex} The rising heating load follows the trend reported by Esmaeili and Pourmoghadam (2023), who found that increased demand leads to lower solar coverage but greater efficiency in exergetic use. The seasonal variations of the annual energy and exergy efficiency values of the collector and the whole system, depending on the dimensionless energy and exergy numbers are shown graphically. In Fig 10a, the energy efficiency of the system reaches a high value of around 93% in June and decreases to its lowest level in December. The energy efficiency of the system shows an increasing trend in the first half of the year and a decreasing trend in the second half. This shows that the system is more efficient in the hot months (June and July) and less efficient in the cold months. In Fig 10b, the exergy efficiency of the system decreases to about 3.2% in January and then increases again in the summer months. Exergy efficiency is higher in the summer months due to the high $\bar{H}_T$ value. The exergy efficiency values of the system exhibit an inverse ratio according to EV_{ex} values. Fig 10c shows that the exergy efficiency of the collector is higher than the exergy efficiency of the whole system. However, the number of EV and EV_{ex} vary inversely with the amounts of energy and exergy efficiency of the system. This new approach can serve as an efficiency benchmark for the system. Our results confirm the findings of Thangavelu et al. (2021) and Gunerhan and Hepbasli (2007), both of whom showed higher collector exergy efficiency in summer and overall system efficiency peaking during high-radiation months. The inverse relation of EV/EV_{ex} to exergy efficiency is similarly noted in their studies.

ERROR ANALYSIS

The present study employs the least-squares fitting of the exergetic fraction value, which is derived from the F-chart method, $f_{ex,F-chart}$ (Eq. (22)), and the actual exergetic fraction value to determine the amount of exergy provided by solar energy to the total exergy demand, $f_{ex,actual}$ (Eq. (26)). The annual resulting changes in these two values are graphically shown in Fig 11. To assess the agreement between the calculated ratio of the amount of exergy provided by solar energy to the total exergy demand. $f_{ex,actual}$ and the value of $f_{ex,F-chart}$, analyzed the difference expression of the two graphs and determined the R^2 values that represent the ratio in the variance of the dependent variable with heating loads considered in Table 6. According to the findings presented in Fig 11, the observed trend indicates a decrease in the difference between the calculated value of $f_{ex,F-chart}$ and the actual value of $f_{ex,actual}$ as the heating load increases. The R^2 values in Table 6 are relatively low, indicating that the model may not accurately capture the variance in the dependent variable concerning heating loads; this trend suggests a strong agreement between the two quantities, as evidenced by the corresponding value obtained. The low R^2 values and trend lines obtained here are comparable to the findings of Bani Yaseen et al. (2020), who also reported close agreement between analytical and simulated exergetic fractions in low-flow solar water systems.

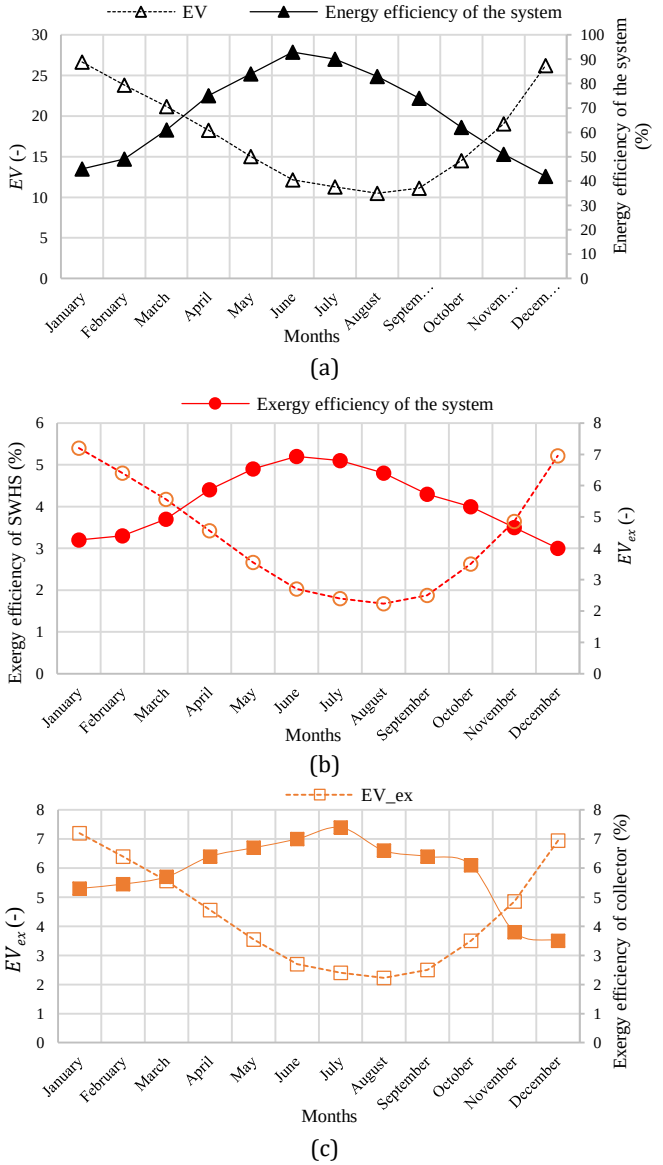

Fig. 10. Comparison of the annual a) energy efficiency of the system, b) exergy efficiency of the system and c) exergy efficiency of the collector according to the number of EV and EV_{ex} .

Table 6. The difference between $f_{ex,F-chart}$, $f_{ex,actual}$ and R^2, the ratio of the dependent variable.

Heating load (GJ)	The difference between the two graphs and R^2, the ratio of the dependent variable	
1	ΔY=0.0005X+0.0599	R^2=0.0248
1.5	ΔY=0.0005X+0.0482	R^2=0.003
3.5	ΔY=0.0004X+0.0311	R^2=0.0028
4	ΔY=0.0004X+0.0221	R^2=0.0011
5	ΔY=0.0003X+0.0185	R^2=0.0008
8	ΔY=0.0002X+0.0119	**R^2=0.0001**

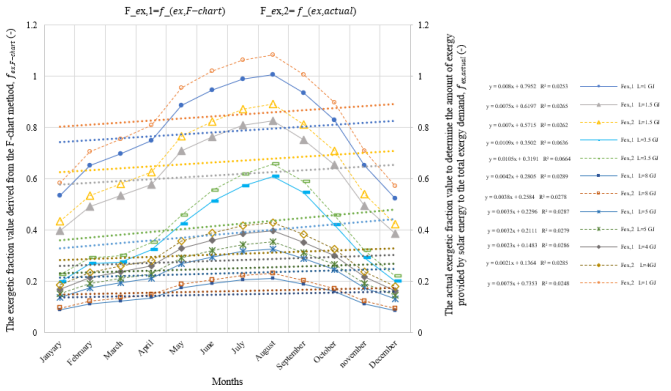

Fig. 11. The annual $f_{ex,F-chart}$ and $f_{ex,actual}$ values for various heating load.

CONCLUSION

This study introduces a novel approach in the field of energy and exergy analysis and optimization of SWH systems. The study is carried out on a theoretically active SWH system in Mugla province using TRNSYS simulation software. By integrating the F-chart method with exergy analysis, new dimensionless energy (EV) and exergy (EV_{ex}) efficiency numbers derived from the F-chart equations are introduced. Furthermore, the solar energy utilization energy ratio (F) and exergetic ratio (F_{ex}) values are calculated. The exergetic utilization ratio represents the contribution of exergy to meeting the heating load of the SWH system, thereby indicating the system's efficiency and how effectively the available solar energy is converted into useful thermal output The analysis results show that the system offers lower F values but higher F_{ex} values. With a 10 m^2 calculated required collector area, the annual F and F_{ex} values are 0.57 and 0.71, respectively. This implies that the energy gain of the system is not completely converted into useful energy (low F), but the amount of usable energy has a significant potential (high F_{ex}). Despite the losses in energy conversion, the remaining energy can be utilized efficiently. A high F_{ex} value indicates that the remaining energy of the system has the potential to perform productive work, while low F values may limit opportunities to fully utilize the energy capacity.

The positive correlation between EV and EV_{ex} numbers reveal that there is a strong relationship between these two values that evaluate the efficiency of the system. According to the results obtained, as the heating load increases, F and F_{ex} values decrease, while EV and EV_{ex} efficiencies increase. For example, at 8 GJ heating load, F and EV are 0.25 and 92.97, respectively, and at 1 GJ heating load they are 0.78 and 11.62. This shows that larger collector areas are required to meet the increasing heating needs and the increase in the heating load directly affects solar energy demand.

The annual energy and exergy efficiencies of the collector and the whole system are evaluated using EV and EV_{ex} values. The analysis shows that energy efficiency increases in the first half of the year and decreases in the second half. It was found that seasonal variations significantly affect the system performance and optimum efficiency is achieved, especially in hot months. In addition, the exergy efficiency of the system increases in the summer months and the high value of $\bar{H}_T$ supports this situation. The exergy efficiency of the collector is higher than the exergy efficiency of the system; both efficiencies exhibit similar changes according to EV_{ex} values. The number of EV and EV_{ex} are inversely proportional to the energy and exergy efficiencies of the system. These numbers can be easily used to measure the energy and exergy efficiencies of SE systems.

According to Fig 8, increasing collector areas increases solar energy utilization rates and exergetic ratio values. However, this increase decreases after a certain size. Smaller collector areas are more effective in maximizing the number of EV and EV_{ex} per unit area. Larger collector areas contribute positively to achieving higher F and F_{ex} values, while smaller collector areas are more effective for maximizing EV and EV_{ex} values. Medium-sized collector areas of approx. 3-4 m^2 offers a balanced solution in all criteria. A collector area of approx. 8 m^2 is recommended for optimum F and F_{ex} performance, while smaller areas of approx. 3-4 m^2 is preferred for unit area efficiency. For balanced performance, medium-sized collector areas should be selected. Ultimately, the ideal size may vary depending on the specific criteria prioritized and the modeling of seasonal conditions. Thus, the optimum system sizing was realized using dimensionless numbers.

For future work, it is recommended to explore various system configurations using hourly dynamic modeling to more accurately demonstrate the potential of the proposed method. Additionally, a comparative analysis involving different types of solar collectors, such as air collectors and vacuum tube collectors, could offer a broader perspective on system performance. Conducting an applied study on residential heating systems would also help validate the method's practical effectiveness. Overall, this study provides a solid foundation for future research in the performance evaluation and optimization of SE systems.

REFERENCES

Abid, M., Yousef, B. A. A., Assad, M. E., Hepbasli, A., & Saeed, K. (2018). An experimental study of solar thermal system with storage for domestic applications. *Journal of Mechanical Engineering and Sciences*, *12*, 4098–4116. https://doi.org/10.15282/jmes.12.4.2018.09.0355

Afzanizam, M., Rosli, M., Shafiq, D., Zaki, M., Rahman, F. A., Sepeai, S., Hamid, N. A., & Nawam, M. Z. (2019). F-Chart Method for Design Domestic Hot Water Heating System in Ayer Keroh Melaka. *Journal of Advanced Research in Fluid Mechanics and Thermal Sciences Journal Homepage*, *56*, 59–67. www.akademiabaru.com/arfmts.html

Agyekum, E. B., Ampah, J. D., Khan, T., Giri, N. C., Hussien, A. G., Velkin, V. I., Mehmood, U., & Kamel, S. (2024). Towards a reduction of emissions and cost-savings in homes: Techno-economic and environmental impact of two

different solar water heaters. *Energy Reports*, *11*, 963–981. https://doi.org/10.1016/j.egyr.2023.12.063

ASHRAE Handbook. (2021). *Service Water Heating*. HVAC Applications, Chapter 49, SI Edition.

Astudillo-Flores, M., Zalamea-Leon, E., Barragán-Escandón, A., Pelaez-Samaniego, M. R., & Calle-Siguencia, J. (2021). Modelling solar thermal energy for household use in equatorial latitude by using the f-chart model. *Renewable Energy and Power Quality Journal*, *19*, 269–275. https://doi.org/10.24084/repqj19.273

Bani Yaseen, A., Al-Hyari, L., Almahmoud, O., & Hammad, M. (2020). Performance of a new solar water heater design with natural circulation. In *Energy Sources, Part A: Recovery, Utilization and Environmental Effects* (pp. 1–16). Taylor and Francis Inc. https://doi.org/10.1080/15567036.2020.1785590

Camargo Nogueira, C. E., Vidotto, M. L., Toniazzo, F., & Debastiani, G. (2016). Software for designing solar water heating systems. In *Renewable and Sustainable Energy Reviews* (Vol. 58, pp. 361–375). Elsevier Ltd. https://doi.org/10.1016/j.rser.2015.12.346

Duffie, J. A., & Beckman, W. A. (2013). *Solar engineering of thermal processes*. Wiley.

Esmaeili, S. M., & Pourmoghadam, P. (2023). Energy exergy and economic evaluation of a CCHP configuration powered by CPVT collectors dynamically. *Energy Reports*, *9*, 6486–6499. https://doi.org/10.1016/j.egyr.2023.06.003

Ghabour, R., & Korzenszky, P. (2021). *Identifying the optimum tilting angles for solar thermal collectors using four different modelling factors in Hungary*. https://www.researchgate.net/publication/363150813

Günerhan, H. (2005, November). *Bir öğrenci yurdu binası için güneş enerjili ve sıvı yakıtlı sıcak su sistemi tasarımı*.

Gunerhan, H., & Hepbasli, A. (2007). Exergetic modeling and performance evaluation of solar water heating systems for building applications. *Energy and Buildings*, *39*(5), 509–516. https://doi.org/10.1016/j.enbuild.2006.09.003

Hepbaşli, A., Günhan Özcan, H., Günerhan, H., & Yildirim, N. (2019, April). *Binaların ekserji bazlı termodinamik analizleri ve değerlendirmeleri*.

Huang, W., & Marefati, M. (2020). Energy, exergy, environmental and economic comparison of various solar thermal systems using water and Thermia Oil B base fluids, and CuO and Al2O3 nanofluids. *Energy Reports*, *6*, 2919–2947. https://doi.org/10.1016/j.egyr.2020.10.021

Jafarkazemi, F., & Ahmadifard, E. (2013). Energetic and exergetic evaluation of flat plate solar collectors. *Renewable Energy*, *56*, 55–63. https://doi.org/10.1016/j.renene.2012.10.031

Jaluria Y. (1998). *Design and Optimization of Thermal Systems*. McGraw-Hill.

Kacia, K., Merzouk, M., Merzouk, N. K., Missoum, M., El Ganaoui, M., Behar, O., & Djedjig, R. (2023). Design, optimization and economic viability of an industrial low temperature hot water production system in Algeria: A case study. *International Journal of Renewable Energy Development*, *12*(3), 448–458. https://doi.org/10.14710/ijred.2023.49759

Kalogirou, S. A., & Florides, G. A. (2016). Solar Space Heating and Cooling Systems☆. In *Reference Module in Earth Systems and Environmental Sciences*. Elsevier. https://doi.org/10.1016/b978-0-12-409548-9.09701-3

Karadağ, B. (2020). *Güneş enerjili su ısıtma sisteminin ekserji ve ekonomik analizi* [Yüksek Lisans Tezi]. Atatürk üniversitesi fen bilimleri enstitüsü.

Kaushik, S. C., & Ranjan, K. R. (2016). Energetic and exergetic performance evaluation of natural circulation solar water heating systems. *Applied Solar Energy (English Translation of Geliotekhnika)*, *52*(1), 16–26. https://doi.org/10.3103/S0003701X16010059

Klein S.A., B. W. A. , and D. J. A. (1975). A Design Procedure For Solar Heating. *Solar Energy, 18, Pp. 113-127*, 113–127.

Kulkarni, M. V., Deshmukh, D. S., & Shekhawat, S. P. (2020). An innovative design approach of hot water storage tank for solar water heating system using artificial neural network. *Materials Today: Proceedings*, *46*, 5400–5405. https://doi.org/10.1016/j.matpr.2020.09.058

Kumar Pathak, S., Tyagi, V. V., Chopra, K., & Kumar Sharma, R. (2022). Recent development in thermal performance of solar water heating (SWH) systems. *Materials Today: Proceedings*, *63*, 778–785. https://doi.org/10.1016/j.matpr.2022.05.502

Meteoroloji Genel Müdürlüğü. (2021). *The highest temperature values in Mugla between 1928-2021*.

Murugan, M., Saravanan, A., Elumalai, P. V., Kumar, P., Ahamed Saleel, C., Samuel, O. D., Setiyo, M., Enweremadu, C. C., & Afzal, A. (2022). An overview on energy and exergy analysis of solar thermal collectors with passive performance enhancers. In *Alexandria Engineering Journal* (Vol. 61, Issue 10, pp. 8123–8147). Elsevier B.V. https://doi.org/10.1016/j.aej.2022.01.052

N. V. Suryanarayana and Öner Arıcı. (2003). *Design and Simulation of Thermal Systems: Vol. TJ260.S87*. McGraw*Hıll.

Okafor, I. F., & Akubue, G. (2012). F-Chart Method for Designing Solar Thermal Water Heating Systems. *International Journal of Scientific & Engineering Research*, *3*(9). http://www.ijser.org

Rincón-Quintero, A. D., Del Portillo-Valdés, L. A., Zanabria-Ortigoza, N. D., Sandoval-Rodriguez, C. L., Maradey-Lázaro, J. G., & Castillo-León, N. Y. (2022). Exergy analysis and development of flat plate solar collectors: A Review. *IOP Conference Series: Materials Science and Engineering*, *1253*(1), 012009. https://doi.org/10.1088/1757-899x/1253/1/012009

S. Klein, et al. (2012). *TRNSYS 17 Manual: A Transient System Simulation Program*. http://sel.me.wisc.edu/trnsys

Savchenko, O., & Savchenko, Z. (2021). Estimation of Solar Hot Water System Operation for a Residential Building. *Energy Engineering and Control Systems*, *7*(1), 1–6. https://doi.org/10.23939/jeecs2021.01.001

Senthil, T. S., Porkodi, M., Ranjith Kumar, R., Vijay Muni, T., Karuna, M. S., & Subbiah, R. (2022). Experimentally Investigating the Flat Plate Solar Water Heating System (FPSWHS) for South Indian Climate. *Journal of Physics: Conference Series*, *2272*(1). https://doi.org/10.1088/1742-6596/2272/1/012010

Thangavelu, S. K., Khoo, R. J., & Piraiarasi, C. (2021). Exergy and exergoeconomic analysis of domestic scale solar water heater by the effect of solar collector area. *Materials Today: Proceedings*, *47*, 5004–5010. https://doi.org/10.1016/j.matpr.2021.04.584

Tiwari, A. K., Gupta, S., Joshi, A. K., Raval, F., & Sojitra, M. (2020). TRNSYS simulation of flat plate solar collector based water heating system in Indian climatic condition. *Materials Today: Proceedings*, *46*, 5360–5365. https://doi.org/10.1016/j.matpr.2020.08.794

TSE 3817. (1994). *General guidelines for solar water heaters*. ICS code: 27.160.

Widén, J., & Munkhammar, J. (2019). Solar Radiation Theory. In *Solar Radiation Theory*. Uppsala University. https://doi.org/10.33063/diva-381852

Zalamea-León, E., Astudillo-Flores, M., Barragán-Escandón, A., & Peláez-Samaniego, M. R. (2023). Comparative capacities of residential solar thermal systems versus F-chart model predictions and economic potential in an equatorial-latitude country. *Energy Reports*, *10*,2567–2581. https://doi.org/10.1016/j.egyr.2023.09.072